Finite element analysis of the transmission characteristics of quantum wires in a magnetic field

Koichi Hirayama*, Yoshihide Taniguchi, Yoshio Hayashi, and Masanori Koshiba

K. Hirayama, Y. Taniguchi, and Y. Hayashi are with the Department of Electrical and Electronic Engineering, Kitami Institute of Technology, Kitami, 090-8507 Japan.

M. Koshiba is with the Division of Electronics and Information Engineering, Hokkaido University, Sapporo, 060-8628 Japan.

*Corresponding author. Tel: +81-157-26-9285; Fax: +81-157-25-1087; e-mail:hira@elec.kitami-it.ac.jp.

abstract

The finite element formulation based on the Galerkin method is proposed for the analysis of the transmission characteristics of quantum wires in a magnetic field. This formulation holds the gauge invariance when the complex conjugate of the wave function is chosen as the test function. Also, it is implied in the formulation that the sum of the outgoing current from a discontinuity region equals the incident current into the region. Moreover, the potential is discretized using the shape function in the quadratic line and triangular elements of the finite element method. If the potential is defined as a quadratic function of the coordinates, it can be exactly described in this discretization, and so this formulation is very suitable for the analysis of realistic quantum wires, whose potential is often expressed with quadratic functions of the coordinates and similar ones. Some discontinuity problems of quantum wires are analyzed and the validity of our approach is shown by comparison with the results of other analysis methods.

keywords

Quantum wire; Parabolic potential; Finite element method;
Transmitted probability; Transmitted current density

1. Introduction

In recent years there has been much interest in investigating the wave nature of electrons and various quantum interference effects in submicron devices. In order to develop quantum devices, it is important to investigate the scattering properties in a quantum waveguide. Especially, the transport properties of quantum devices in a magnetic field are much interesting, and various analysis methods for arbitrarily shaped quantum devices such as the boundary-element method (BEM) [1], the finite element method (FEM), [2,3], and the finite difference method (FDM) [4] have been developed. In Ref. [1], an exact but complicated Green's function has been developed, and wave functions have been calculated using the BEM for a charged particle injected into a semi-infinite two-dimensional region consisting of a quantum wire in a perpendicular magnetic field. In Ref. [4], the effects of a perpendicular magnetic field on a closed stadium-shaped cavity was studied using the FDM. Also, the approaches based on the recursive Green's-function method (RGM) have been developed for the analysis of the transmission characteristics of quantum wires with a parabolic-type potential in a magnetic field [5,6].

Using the FEM, a stadium-shaped quantum dot [2] and a quantum wire involving a single antidot [3] are analyzed. Previously we proposed a novel finite element formulation for the analysis of the energy levels of a two-dimensional quantum cavity in a magnetic field [7]. In the formulation of Ref. [7], the final eigenvalue matrix equation consists of a real symmetric and an Hermitian matrix, while that of Refs. [2] and [3] would generate asymmetric (neither real symmetric nor Hermitian) matrices for a cavity in a magnetic field. The FEM which is based on the variational method and generates Hermitian matrices has been proposed for a four band **k-p** analysis on the valence band structure of a quantum wire [8], but it does not contain the analysis of a quantum wire in a magnetic field.

In this paper, we apply the formulation based on the Galerkin method in Ref. [7] to the analysis of the transmission characteristics of quantum wires in a magnetic field. The Schrödinger equation is invariant in gauge transform, and our formulation holds the gauge invariance when the complex conjugate of the wave function is chosen as the test function, while that in Refs. [2] and [3] does not. Also, it is implied in our formulation that the sum of the outgoing current from a discontinuity region equals the incident current into the region. Moreover, the potential as well as the wave function is discretized using the shape function in the quadratic line and triangular elements of the FEM, since realistic quantum wires may have a potential profile which changes in a complicated fashion as a function of the position.

If the potential is defined as a quadratic function of the coordinates, it can be exactly described in this discretization, and so this formulation is very suitable for the analysis of realistic quantum wires, whose potential is often expressed with quadratic functions of the coordinates and similar ones [5].

2. Theoretical Formulation

2.1. Basic equation

We consider a two-dimensional discontinuity problem of quantum wires, as shown in Fig. 1, where Γ_0 is a hard wall (the barrier along Γ_0 is infinitely high) and Γ_j $(j = 1, 2, \cdots, N)$ connects the discontinuity region Ω to the infinite uniform wire j. We assume that a uniform perpendicular magnetic field $\mathbf{B} = \hat{z}B$ is applied over region Ω and the wires, where $\mathbf{B}$ is the magnetic-flux density vector, B is a constant, and $\hat{z}$ is the unit vector in the z direction. Since the z confinement is stronger, we neglect its contribution and zero energy is taken as the edge of the fundamental z-related subband without any loss of generality. Under the effective-mass approximation, the time-independent Schrödinger equation is given by

$$\left[\frac{1}{2m}(-i\hbar\nabla + e\mathbf{A})^2 + V\right]\psi = E\psi \tag{1}$$

where m, $-e$, E, and ψ are the electron effective mass, charge, total energy, and envelop wave function, respectively, and the effective mass is assumed to be uniform in Ω and the wires. The symbols $\mathbf{A}$ and V denote the vector potential and the potential energy, respectively, and $\hbar$ is Plank's constant divided by 2π. With the choice of the Coulomb's gauge $\nabla \cdot \mathbf{A} = 0$, applying the Galerkin method to Eq. (1), we obtain the following equation [7]:

$$\begin{aligned}
&\iint_\Omega \left\{\nabla\bar{\psi}\cdot\nabla\psi - i\frac{e}{\hbar}(\mathbf{A}\bar{\psi})\cdot(\nabla\psi) + i\frac{e}{\hbar}(\nabla\bar{\psi})\cdot(\mathbf{A}\psi)\right.\\
&\left.+\left[\left(\frac{e\mathbf{A}}{\hbar}\right)^2 + \frac{2mV}{\hbar^2} - k^2\right]\bar{\psi}\psi\right\}dxdy\\
&= \sum_{j=1}^{N}\int_{\Gamma_j}\bar{\psi}_j\left(\nabla\psi_j + i\frac{e}{\hbar}\mathbf{A}\psi_j\right)\cdot\hat{x}_j dy_j
\end{aligned} \tag{2}$$

where $k^2 = 2mE/\hbar^2$, $\bar{\psi}$ is a test function, and $\hat{x}_j$ is the outward unit vector normal to Γ_j. The integral $\iint_\Omega dxdy$ represents the area integration over Ω, and $\int_{\Gamma_j} dy_j$ represents the line integration over Γ_j.

For $\bar{\psi} = \psi^*$ (ψ^* being the complex conjugate of ψ), we notice that the integrands in the left- and right-hand sides of Eq. (2) are invariant in the following gauge transform:

$$\psi = e^{-ie\Lambda/\hbar}\psi', \quad \mathbf{A} = \mathbf{A}' + \nabla\Lambda \tag{3}$$

where Λ is an arbitrary scalar function, and the wave functions ψ and ψ' are for the vector potentials $\mathbf{A}$ and $\mathbf{A}'$, respectively. Unfortunately, the formulations published previously (Eq. (7) of Ref. [2] and Eq. (33) of Ref. [3]) do not hold the gauge invariance. Also, since the current density is defined as

$$\mathbf{J} = \frac{\hbar}{m}\,\mathrm{Im}\left[\psi^*\left(\nabla\psi + i\frac{e}{\hbar}\mathbf{A}\psi\right)\right] \tag{4}$$

the imaginary part of the right-hand side of Eq. (2) is written as

$$\frac{m}{\hbar}\sum_{j=1}^{N}\int_{\Gamma_j}\mathbf{J}_j\cdot\hat{x}_j dy_j = \frac{m}{\hbar}\left(\sum_{j=1}^{N} I_j - I_{\mathrm{inc}}\right) \tag{5}$$

where I_{inc} represents the incident current and I_j is the outgoing current into the wire j. The value of this expression must be zero because the left-hand side of Eq. (2) is a real number for $\bar{\psi} = \psi^*$, and it corresponds directly to the fact that the sum of the outgoing current equals the incident current.

2.2. Finite element discretization

We divide region Ω into a number of quadratic triangular elements [9] and discretize the envelop wave function and the potential in the element as

$$\psi = \{N\}^T\{\psi\}_e, \quad \bar{\psi} = \{N\}^T\{\bar{\psi}\}_e, \quad V = \{N\}^T\{V\}_e \tag{6}$$

where the components of the vectors $\{\psi\}_e$, $\{\bar{\psi}\}_e$, and $\{V\}_e$ are the values of ψ, $\bar{\psi}$, and V at the nodes in the element, respectively, $\{N\}$ is the shape function vector [9], and the superscript T denotes transpose. Substituting Eq. (6) into Eq. (2), we can obtain the following equation:

$$\{\bar{\psi}\}^T[P]\{\psi\} = \sum_{j=1}^{N}\int_{\Gamma_j}\bar{\psi}_j\left(\nabla\psi_j + i\frac{e}{\hbar}\mathbf{A}\psi_j\right)\cdot\hat{x}_j dy_j \tag{7}$$

with

$$[P] \;=\; \sum_e \iint_e \left\{ \frac{\partial\{N\}}{\partial x}\frac{\partial\{N\}^T}{\partial x} + \frac{\partial\{N\}}{\partial y}\frac{\partial\{N\}^T}{\partial y}\right.$$

$$
\begin{aligned}
&-i\frac{e}{\hbar}\left(\{N\}A_x\frac{\partial\{N\}^T}{\partial x}+\{N\}A_y\frac{\partial\{N\}^T}{\partial y}\right)\\
&+i\frac{e}{\hbar}\left(\frac{\partial\{N\}}{\partial x}A_x\{N\}^T+\frac{\partial\{N\}}{\partial y}A_y\{N\}^T\right)\\
&+\left[\left(\frac{e\mathbf{A}}{\hbar}\right)^2+\frac{2m}{\hbar^2}\{N\}^T\{V\}_e-k^2\right]\{N\}\{N\}^T\Bigg\}dxdy
\end{aligned}
$$

where the components of the vectors $\{\psi\}$ and $\{\bar{\psi}\}$ are the values of ψ and $\bar{\psi}$ at all the nodes except those on boundary Γ_0, respectively, $[P]$ is a sparse Hermitian matrix, A_x and A_y are the x and y components of $\mathbf{A}$, respectively, $\iint_e dxdy$ represents the area integration over an element, and $\sum_e$ stands for the sum over all the elements in region Ω.

2.3. Analytical relations

We choose the vector potential $\mathbf{A}'_j=-\hat{x}_jBy_j$ in wire j and the envelop wave function ψ'_j for $\mathbf{A}'_j$. We can set $\psi_j=e^{-ie\Lambda_j/\hbar}\psi'_j$, where $\nabla\Lambda_j=\mathbf{A}-\mathbf{A}'_j$, and then the integral of the right-hand side of Eq. (7) may be reduced as

$$
\int_{\Gamma_j}\bar{\psi}_j\left(\nabla\psi_j+i\frac{e}{\hbar}\mathbf{A}\psi_j\right)\cdot\hat{x}_jdy_j=\int_{\Gamma_j}\bar{\psi}_je^{-ie\Lambda_j^0/\hbar}\left(\frac{\partial\psi'_j}{\partial x_j}-i\frac{y_j}{l_B^2}\psi'_j\right)dy_j \tag{8}
$$

where $\Lambda_j^0=\Lambda_j(x_j=0,y_j)$ and $l_B=\sqrt{\hbar/eB}$ represents a magnetic length.

When the incident wave of a propagating mode with unity amplitude comes from wire 1, the wave function ψ'_j in wire j is expressed as

$$
\psi'_j(x_j,y_j)=\delta_{j1}e^{-i\beta_{\rm inc}x_1}f_{\rm inc}(y_1)+\sum_{n=1}^{\infty}b_{jn}e^{i\beta_{jn}x_j}f_{jn}(y_j) \tag{9}
$$

and

$$
\left.\frac{\partial\psi'_j}{\partial x_j}-i\frac{y_j}{l_B^2}\psi'_j\right|_{\Gamma_j}=\delta_{j1}g_{\rm inc}(y_1)+\{g_j(y_j)\}^T\{b_j\} \tag{10}
$$

with

$$
\begin{aligned}
g_{\rm inc}(y_1) &= \left(-i\beta_{\rm inc}-i\frac{y_1}{l_B^2}\right)f_{\rm inc}(y_1)\\
\{g_j(y_j)\}_n &= \left(i\beta_{jn}-i\frac{y_j}{l_B^2}\right)f_{jn}(y_j)\equiv g_{jn}(y_j)\\
\{b_j\}_n &= b_{jn}
\end{aligned}
$$

where β_{jn} and $f_{jn}(y_j)$ stand for the phase constant and the mode function of the mth mode in wire j, respectively, and $\beta_{\rm inc}$ and $f_{\rm inc}(y_1)$ represent those of the incident mode. Here $\{\cdot\}_n$ is the nth component of the corresponding column vector, and δ_{j1} is the Kronecker's delta. We can not always obtain β_{jn} and $f_{jn}(y_j)$ analytically, so we calculate them numerically by use of the FEM, as described in Appendix. Multiplying Eq. (9) with $f^*_{jl}(y_j)$ $(l = 1, 2, \cdots)$ and integrating the equation over Γ_j, we can obtain

$$\{b_j\} = [H_j]^{-1} \int_{\Gamma_j} \{f_j(y_j)\}^* [-\delta_{j1} f_{\rm inc}(y_1) + e^{ie\Lambda^0_j/\hbar}\psi_j] dy_j \tag{11}$$

with

$$\{f_j(y_j)\}_n = f_{jn}(y_j), \quad [H_j]_{ln} = \int_{\Gamma_j} f^*_{jl}(y_j) f_{jn}(y_j) dy_j$$

where the superscript $*$ stands for the complex conjugate, and $[\cdot]_{ln}$ is the lth-row and nth-column component of the corresponding matrix. We divide boundary Γ_j into a number of quadratic line elements [9] and discretize the envelop wave function on Γ_j as

$$\psi_j = \{N_j\}^T \{\psi_j\} \tag{12}$$
$$\bar{\psi}_j = \{N_j\}^T \{\bar{\psi}_j\} \tag{13}$$

where the components of the vectors $\{\psi_j\}$ and $\{\bar{\psi}_j\}$ are the values of ψ and $\bar{\psi}$ at the nodes on Γ_j, respectively, and $\{N_j\}$ is the shape function vector along Γ_j. Substituting Eq. (12) into Eq. (11), $\{b_j\}$ is given as

$$\{b_j\} = -\delta_{j1}[H_1]^{-1}\{F_{\rm inc}\} + [H_j]^{-1}[F_j]\{\psi_j\} \tag{14}$$

with

$$\{F_{\rm inc}\} = \int_{\Gamma_1} \{f_1(y_1)\}^* f_{\rm inc}(y_1) dy_1, \quad [F_j] = \int_{\Gamma_j} \{f_j(y_j)\}^* e^{ie\Lambda^0_j/\hbar} \{N_j\}^T dy_j$$

We finally obtain from Eqs. (8), (10), (13), and (14)

$$\int_{\Gamma_j} \bar{\psi}_j \left(\nabla\psi_j + i\frac{e}{\hbar}\mathbf{A}\psi_j \right) \cdot \hat{x}_j dy_j = \delta_{j1}\{\bar{\psi}_1\}^T\{\Psi_{\rm inc}\} - \{\bar{\psi}_j\}^T[Z_j]\{\psi_j\} \tag{15}$$

with

$$\{\Psi_{\rm inc}\} = \{G_{\rm inc}\} - [G_1][H_1]^{-1}\{F_{\rm inc}\}, \quad [Z_j] = -[G_j][H_j]^{-1}[F_j]$$

where

$$\{G_{\rm inc}\} = \int_{\Gamma_1} \{N_1\} e^{-ie\Lambda^0_1/\hbar} g_{\rm inc}(y_1) dy_1, \quad [G_j] = \int_{\Gamma_j} \{N_j\} e^{-ie\Lambda^0_j/\hbar} \{g_j(y_j)\}^T dy_j$$

2.4. Evaluation of transmitted probability

Using Eqs. (7) and (15), we can obtain the following matrix equation:

$$\begin{bmatrix} [P_{00}] & [P_{01}] & [P_{02}] & \cdots & [P_{0N}] \\ [P_{10}] & [P_{11}]+[Z_1] & [P_{12}] & \cdots & [P_{1N}] \\ [P_{20}] & [P_{21}] & [P_{22}]+[Z_2] & \cdots & [P_{2N}] \\ \vdots & \vdots & \vdots & \ddots & \vdots \\ [P_{N0}] & [P_{N1}] & [P_{N2}] & \cdots & [P_{NN}]+[Z_N] \end{bmatrix} \begin{bmatrix} \{\psi_0\} \\ \{\psi_1\} \\ \{\psi_2\} \\ \vdots \\ \{\psi_N\} \end{bmatrix} = \begin{bmatrix} \{0\} \\ \{\Psi_{\rm inc}\} \\ \{0\} \\ \vdots \\ \{0\} \end{bmatrix} \tag{16}$$

where the components of the vector $\{\psi_0\}$ are the values of the nodes in region Ω except the nodes on boundary Γ_j. This final matrix equation has a sparse complex (neither symmetric nor Hermitian) matrix, and may be solved efficiently by using the bi-conjugate gradient method with the precondition of the incomplete LU decomposition.

The current density across Γ_j is given as

$$\begin{aligned} \mathbf{J}_j \cdot \hat{x}_j|_{\Gamma_j} &= \frac{\hbar}{m}{\rm Im}\left[\psi_j'^{*}\left(\frac{\partial\psi_j'}{\partial x_j} - i\frac{y_j}{l_B^2}\psi_j'\right)\Big|_{\Gamma_j}\right] \\ &= \delta_{j1}\frac{\hbar}{m}\left[-\left(\beta_{\rm inc}+\frac{y_1}{l_B^2}\right)f_{\rm inc}^2(y_1)\right. \\ &\quad \left. + \sum_{n=1}^{M_1}{\rm Re}[b_{1n}]\left(-\beta_{\rm inc}+\beta_{1n}-\frac{2y_1}{l_B^2}\right)f_{\rm inc}(y_1)f_{1n}(y_1)\right] \\ &\quad + \frac{\hbar}{2m}\sum_{l=1}^{M_j}\sum_{n=1}^{M_j} b_{jl}^{*}b_{jn}\left(\beta_{jl}+\beta_{jn}-\frac{2y_j}{l_B^2}\right)f_{jl}(y_j)f_{jn}(y_j) \end{aligned} \tag{17}$$

where M_j represents the number of the propagating modes in wire j, and Re[$\cdot$] and Im[$\cdot$] denote the real and imaginary parts of a complex number, respectively. Using the orthogonality relation Eq. (A.6), we derive

$$\int_{\Gamma_j}\mathbf{J}_j\cdot\hat{x}_j dy_j = -\delta_{j1}I_{\rm inc} + I_j \tag{18}$$

with

$$I_{\rm inc} = \frac{\hbar}{m}\int_{\Gamma_1}\left(\beta_{\rm inc}+\frac{y_1}{l_B^2}\right)f_{\rm inc}^2(y_1)dy_1$$

$$I_j = \frac{\hbar}{m} \sum_{n=1}^{M_j} |b_{jn}|^2 \int_{\Gamma_j} \left(\beta_{jn} - \frac{y_j}{l_B^2} \right) f_{jn}^2(y_j) dy_j$$

After solving Eq. (16) and determining $\{b_j\}$ from Eq. (14), we can finally obtain the transmitted probability of wire j as $T_j = I_j / I_{\rm inc}$.

3. Numerical Examples

In order to show the validity and the usefulness of our approach, we analyze some discontinuity problems of quantum wires.

First we consider a quantum wire with a circular antidot in a magnetic field, as shown in Fig. 2, where d is the width of the wire, D is the diameter of the antidot, and boundaries Γ_1, Γ_2 are located at $x = -a$, a, respectively. Here $a/d = 1.5$, $D/d = 0.1$, and the magnetic length is $l_B = d/\sqrt{22.8}$ [3]. The potential V is set equal to zero in the discontinuity region and the wires. The antidot is replaced with an equilateral 32-side polygon of an area equal to the original circular one. Figure 3 shows the transmitted probability against the change of the electron energy for the first-mode or second-mode incidence, where the electron energy is normalized by $E_0 = (\hbar^2/2m)(\pi/d)^2$. For $E/E_0 < 2.35$, no propagating mode exists. Figure 4 shows the probability density in contour lines and the probability current density in arrows at $E/E_0 = 4.37$ where the transmitted probability is nearly equal to zero. Here we take into account one propagating and nine non-propagating modes for $E/E_0 < 7.28$ and two propagating and eight non-propagating ones for $E/E_0 \geq 7.28$ in each of wires 1 and 2. Our results agree well with those of Leng et al. [3].

Next we consider a quantum wire with a parabolic potential in a magnetic field, as shown in Fig. 5, where the potential profile is given as

$$V(y) = \begin{cases} V_w(y) = m\omega_w^2 y^2/2, & |x| > b/2 \\ V_s(y) = m\omega_s^2 y^2/2, & |x| \leq b/2 \end{cases}$$

Here we assume $b = 40\,\mathrm{nm}$, $B = 0$ or $0.3\,\mathrm{T}$, $\hbar\omega_w = 6.39\,\mathrm{meV}$, $E = 9\,\mathrm{meV}$ [6], and $m = 0.067 m_0$ (m_0 being the electron mass in free space). In order to analyze this discontinuity problem by using the FEM formulated in the previous section, we put hard walls at $y = \pm d/2$, whose barriers are infinitely high and then the discontinuity region Ω is defined as the rectangular region of $(|x| \leq a + b/2) \wedge (|y| \leq d/2)$. We set $a = 100\,\mathrm{nm}$ and $d = 360\,\mathrm{nm}$, and take into account one propagating mode and nine non-propagating modes in each of wires 1 and 2.

Figure 6 shows the transmitted probability and the phase of the propagating mode against the change of the potential V_s for $B = 0$. Here the reference

plane of the phase is located at $x = -b/2$ for the incident propagating mode and $x = b/2$ for the transmitted one. We find that at $\omega_w/\omega_s = 2.26$, 4.37, and 6.65, the transmitted probability is zero and the phase changes dramatically by 2π. If we do not put the hard walls at $y = \pm d/2$, we can analytically obtain the propagating and non-propagating modes in each of the regions of the potentials V_w and V_s, and then we may calculate the transmitted probability by using the mode-matching method (MMM). The dark dots in Fig. 6 present the results of the MMM. The computed results of the FEM and the MMM are in good agreement, and so we confirm that the hard walls at $y = \pm d/2$ do not affect the results and the results of the FEM is in good accuracy.

Figure 7 shows the transmitted probability and the phase of the propagating mode in wire 2 against the change of the potential V_s for $B = 0.3\,\mathrm{T}$. The computed results of the FEM and the MMM are in good agreement, but unfortunately we were not able to calculate the transmitted probability for $\omega_w/\omega_s > 3$ by using the MMM, because the sum of the transmitted probability was not unity even if we took into account 50 non-propagating modes in each of the regions of the potentials V_w and V_s.

Finally we consider a T-junction quantum wire in a magnetic field, as shown in Fig. 8, where d is the width of wire 1, D is that of wires 2 and 3, Γ_1 is located at $y = -D/2 - a$, and Γ_2, Γ_3 are located at $x = -d/2 - b$, $d/2 + b$, respectively. The intensity of the magnetic field is given as $R_c/\lambda_F = 10$, where $\lambda_F = 2\pi/k$ is the Fermi wavelength and $R_c = kl_B^2$ is the cyclotron radius. We take into account 20 modes (all the propagating modes and some non-propagating ones) in each of wires 1 to 3.

We assume that $d/\lambda_F = 2.1$, $a/\lambda_F = 1$, $b/\lambda_F = 10$, and the potential V is set equal to zero in the discontinuity region and the wires. Figure 9 shows the sum of the transmitted probability of wires 2 and 3 against the change of the width of wires 2 and 3 for the first- or second-mode incidence from wire 1. In comparison with those of RGM [5], our results are in good agreement for the first-mode incidence, and somewhat greater for the second-mode incidence.

We can treat the parabolic-type potential profile in Ref. [5], as shown in Fig. 10, given as

$$V/E = [x^2 - (c_x - R)^2]/\lambda_F^2 + 1$$

in Region I,

$$V/E = (r - R)\left[\left(1 - \frac{2c_x}{c_x - |x|}\right) r + R\right]/\lambda_F^2 + 1$$

in Region II,

$$V/E = (R + \lambda_F - r)^2/\lambda_F^2$$

for $r < R + \lambda_F$ and zero for $r \geq R + \lambda_F$ in Region III, and

$$V/E = (|y| - c_y + R + \lambda_F)^2/\lambda_F^2$$

for $|y| > c_y - R - \lambda_F$ and zero for $|y| \leq c_y - R - \lambda_F$ in Region IV. Here $c_x = c + d/2$, $c_y = c + D/2$, and $r = \sqrt{(c_x - |x|)^2 + (c_y + y)^2}$. Regions I and IV are defined as $y \leq -c_y$ and $(|x| \geq c_x) \vee (y \geq 0)$, respectively, and the region $(|x| < c_x) \wedge (-c_y < y < 0)$ is divided into regions II and III at the two lines between the points of $(\pm c_x, -c_y)$ and $(0, -c_y + \sqrt{(R + \lambda_F)^2 - c_x^2})$. The potential V in region III is set equal to the electron energy E at $r = R$ and zero at $r = R + \lambda_F$. The parameters of the length should satisfy the relation $R < c_x < R + \lambda_F \leq c_y$. For $R/\lambda_F = 6.2$, we assume $c/\lambda_F = 4$ and $d/\lambda_F = 6.1$, while $c/\lambda_F = 3$ and $d/\lambda_F = 8.1$ are used in Ref. [5], because we confirmed in the numerical investigation that the case of $c/\lambda_F = 4$ and $d/\lambda_F = 6.1$ yields almost the same results as the other in less computational time. Also, we set $a/\lambda_F = b/\lambda_F = 5$. Figure 11 shows the sum of the transmitted probability of wires 2 and 3 against the change of the width of wires 2 and 3 for the first- or second-mode incidence from wire 1. Our results agree approximately both for the first- and second-mode incidence with those of RGM [5]. We believe that our results are more correct, because the parabolic-type potential is expressed with quadratic functions of the coordinates in an triangular element in the FEM, while only with the values at the vertices of a square lattice in the RGM. Figure 12 shows the probability density in contour lines and the probability current density in arrows at $D/\lambda_F = 8$ for the first-mode incidence. We find that the electron wave is well confined in the region within the broken lines for $V = E$, which present the wire configuration in classical mechanics.

4. Conclusion

The finite element formulation based on the Galerkin method has been proposed for the analysis of the transmission characteristics of quantum wires in a magnetic field. This formulation holds the gauge invariance, and it is implied that the sum of the outgoing current from a discontinuity region equals the incident current into the region. Also, the potential is discretized using the shape function in the quadratic line and triangular elements of the FEM in order to treat realistic quantum wires with a potential profile which changes in a complicated fashion as a function of the position. We have analyzed a quantum wire with a circular antidot or a parabolic potential and a T-junction quantum wire with zero or a parabolic-type potential, and have

shown the validity of our approach by comparison with the results of other analysis methods.

In the future, we shall investigate in detail the effects of the shape of a quantum wire, the profile of a potential, etc. on the transmission characteristics of quantum wires in a magnetic field by using the finite element analysis proposed here.

Appendix

When we set the wave function as $\psi'_j = e^{i\beta_j x_j} f_j(y_j)$ for the vector potential $\mathbf{A}'_j = -\hat{x}_j B y_j$ in wire j, we obtain the following equation from Eq. (1):

$$\frac{d^2 f_j}{dy_j^2} + \left[k^2 - \frac{2mV_j(y_j)}{\hbar^2} - \left(\frac{y_j}{l_B^2} - \beta_j \right)^2 \right] f_j(y_j) = 0 \tag{A.1}$$

Under the boundary condition $f_j(\pm d_j/2) = 0$, the functional for Eq. (A.1) is given as

$$F(f_j) = \frac{1}{2} \int_{\Gamma_j} \left\{ \left(\frac{df_j}{dy_j} \right)^2 - \left[k^2 - \frac{2mV_j(y_j)}{\hbar^2} - \left(\frac{y_j}{l_B^2} - \beta_j \right)^2 \right] f_j^2(y_j) \right\} dy_j \tag{A.2}$$

We divide boundary Γ_j into a number of quadratic line elements and discretize $f_j(y_j)$ and $V_j(y_j)$ on Γ_j as

$$f_j(y_j) = \{N_j\}^T \{f_j\}, \quad V_j(y_j) = \{N_j\}^T \{V_j\} \tag{A.3}$$

where the components of the vectors $\{f_j\}$ and $\{V_j\}$ are the values of $f_j(y_j)$ and $V_j(y_j)$ at the nodes on Γ_j. Substituting Eq. (A.3) into Eq. (A.2) and applying the variational principle, we obtain the following eigenvalue equation:

$$\begin{bmatrix} [Q_1] & [Q_0] \\ [1] & [0] \end{bmatrix} \begin{bmatrix} \beta_j \{f_j\} \\ \{f_j\} \end{bmatrix} = \beta_j \begin{bmatrix} [Q_2] & [0] \\ [0] & [1] \end{bmatrix} \begin{bmatrix} \beta_j \{f_j\} \\ \{f_j\} \end{bmatrix} \tag{A.4}$$

with

$$\begin{aligned} [Q_0] &= \int_{\Gamma_j} \left[-\frac{d\{N_j\}}{dy_j} \frac{d\{N_j\}^T}{dy_j} + \left(k^2 - \frac{2m}{\hbar^2} \{N_j\}^T \{V_j\} - \frac{y_j^2}{l_B^4} \right) \{N_j\} \{N_j\}^T \right] dy_j \\ [Q_1] &= \int_{\Gamma_j} \frac{2y_j}{l_B^2} \{N_j\} \{N_j\}^T dy_j \\ [Q_2] &= \int_{\Gamma_j} \{N_j\} \{N_j\}^T dy_j \end{aligned}$$

where [0] and [1] are the null and unit matrix, respectively. We can obtain the phase constants and the mode functions from the solution of Eq. (A.4).

For the lth and nth modes in wire j, we can derive from Eq. (A.1)

$$\begin{aligned} &\frac{d}{dy_j} \left[f_{jl}(y_j) \frac{df_{jn}}{dy_j} - f_{jn}(y_j) \frac{df_{jl}}{dy_j} \right] \\ &+ \left[-\left(\frac{y_j}{l_B^2} - \beta_{jn} \right)^2 + \left(\frac{y_j}{l_B^2} - \beta_{jl} \right)^2 \right] f_{jl}(y_j) f_{jn}(y_j) = 0 \end{aligned} \tag{A.5}$$

Integrating this equation over Γ_j, we can obtain the following orthogonality relation [10]:

$$(\beta_{jl} - \beta_{jn}) \int_{\Gamma_j} \left(\beta_{jl} + \beta_{jn} - \frac{2y_j}{l_B^2} \right) f_{jl}(y_j) f_{jn}(y_j) dy_j = 0 \qquad \text{(A.6)}$$

References

[1] T. Ueta, Green's function of a charged particle in magnetic fields, J. Phys. Soc. Jpn. 61 (1992) 4314–4324.

[2] Y. Wang, J. Wang, H. Guo, Magnetoconductance of a stadium-shaped quantum dot: A finite-element-method approach, Phys. Rev. B 49 (1994) 1928–1934.

[3] M. Leng, C. S. Lent, Quantum transmitting boundary method in a magnetic field, J. Appl. Phys. 76 (1994) 2240–2248.

[4] Z.-L. Ji, K.-F. Berggren, Transition from chaotic to regular behavior of electrons in a stadium-shaped quantum dot in a perpendicular magnetic field, Phys. Rev. B 52 (1995) 1745–1750.

[5] T. Usuki, M. Saito, M. Takatsu, R. A. Kiehl, N. Yokoyama, Numerical analysis of ballistic-electron transport in magnetic fields by using a quantum point contact and a quantum wire, Phys. Rev. B 52 (1995) 8244–8255.

[6] R. Akis, P. Vasilopoulos, P. Debray, Bound states and transmission antiresonances in parabolically confined cross structures: Influence of weak magnetic fields, Phys. Rev. B 56 (1997) 9594–9602.

[7] K. Hirayama, Y. Honma, Y. Hayashi, M. Koshiba, A novel finite-element formulation for the analysis of the energy levels of a quantum cavity in a magnetic field, IEEE Photon. Technol. Lett. 10 (1998) 1359–1361.

[8] J. C. Yi, N. Dagli, Finite-element analysis of valence band structure and optical properties of quantum-wire arrays on vicinal substrates, IEEE J. Quantum Electron. 31 (1995) 208–218.

[9] M. Koshiba, Optical Waveguide Theory by the Finite Element Method, Tokyo/Dordrecht: KTK Scientific Publishers/Kluwer Academic Publishers, 1992.

[10] R. L. Schult, H. W. Wyld, D. G. Ravenhall, Quantum Hall effect and general narrow-wire circuits, Phys. Rev. B 41 (1990) 12760–12780.

Figure Captions

Fig. 1. Discontinuity of quantum wires in a perpendicular magnetic field.
Fig. 2. Quantum wire with a circular antidot, where $a/d = 1.5$, $D/d = 0.1$, the magnetic length is $l_B = d/\sqrt{22.8}$, and the potential is $V = 0$.
Fig. 3. Transmitted probability for a quantum wire with a circular antidot, where $E_0 = (\hbar^2/2m)(\pi/d)^2$.
Fig. 4. Probability density (contour lines) and probability current density (arrows) at $E/E_0 = 4.37$ for a quantum wire with a circular antidot.
Fig. 5. Quantum wire with a parabolic potential, where $a = 100\,\mathrm{nm}$, $b = 40\,\mathrm{nm}$, $d = 360\,\mathrm{nm}$, the factor of the potential in a semi-infinite uniform wire is $\hbar\omega_w = 6.39\,\mathrm{meV}$, the electron energy is $E = 9\,\mathrm{meV}$, and the electron effective mass is $m = 0.067m_0$ (m_0 being the electron mass in free space).
Fig. 6. Transmitted probability and phase of the propagating mode for a quantum wire with a parabolic potential in $B = 0$.
Fig. 7. Same as Fig. 6, but in $B = 0.3\,\mathrm{T}$.
Fig. 8. T-junction quantum wire, where $a/\lambda_F = 1$, $b/\lambda_F = 10$, $d/\lambda_F = 2.1$, and the cyclotron radius is $R_c = 10\lambda_F$ (λ_F being the Fermi wavelength).
Fig. 9. Transmitted probability of a T-junction quantum wire for the first- or second-mode incidence in $V = 0$.
Fig. 10. Parabolic-type potential profile in a T-junction quantum wire. The broken lines for $V = E$ present the wire configuration in classical mechanics.
Fig. 11. Same as Fig. 9, but in the parabolic-type potential.
Fig. 12. Probability density (contour lines) and probability current density (arrows) at $D/\lambda_F = 8$ for the first-mode incidence in a T-junction quantum wire with a parabolic-type potential.

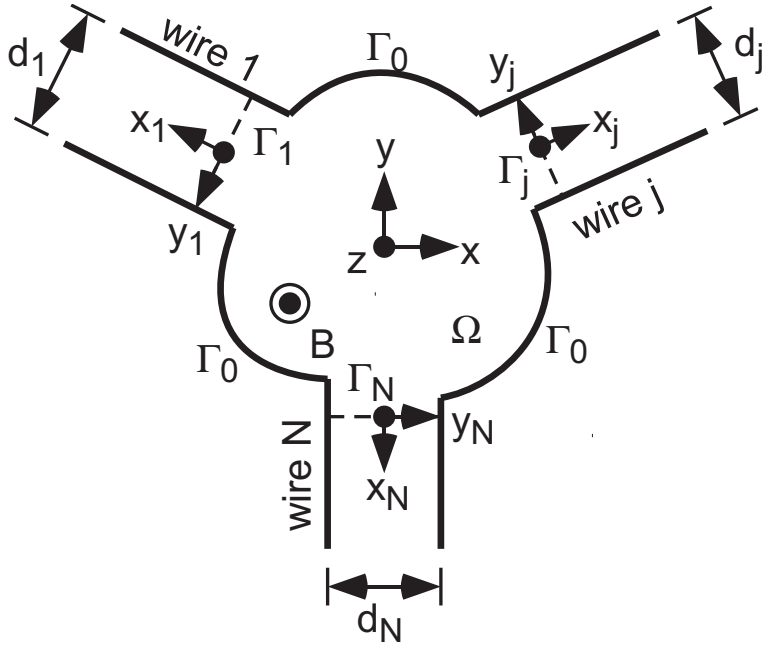
d1
wire 1
Γ0
yj
dj
x1
Γ1
xj
Γj
y
z
x
wire j
y1
B
Ω
Γ0
Γ0
ΓN
yN
wire N
xN
dN

Fig. 1

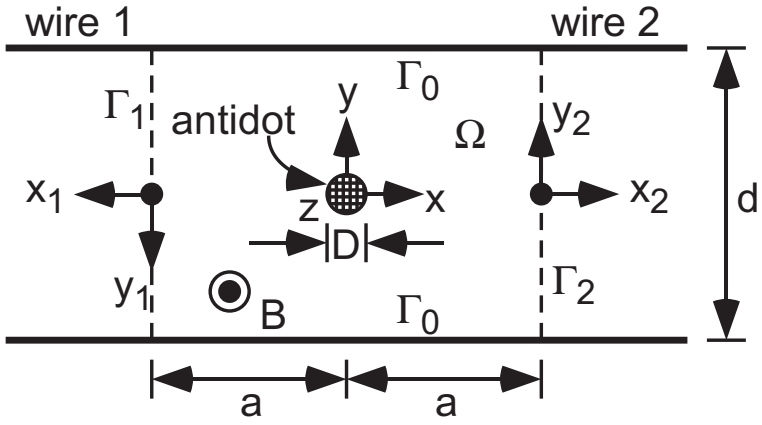
wire 1
wire 2
Γ0
Γ1
antidot
y
Ω
y2
x1
z
x
x2
d
D
y1
B
Γ0
Γ2
a
a

Fig. 2

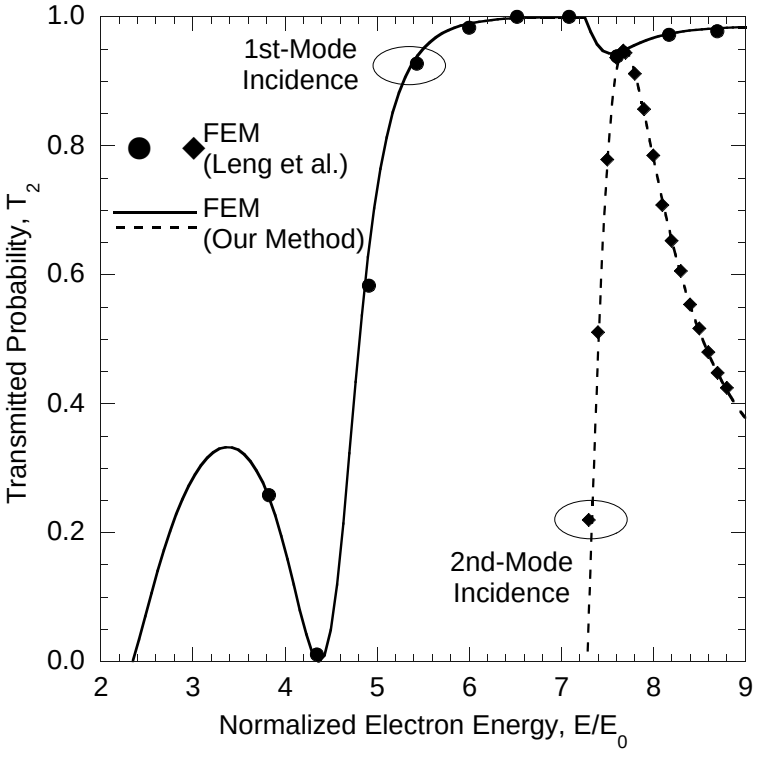
1st-Mode
Incidence
FEM
(Leng et al.)
FEM
(Our Method)
2nd-Mode
Incidence
Transmitted Probability, T2
Normalized Electron Energy, E/E0
1.0
0.8
0.6
0.4
0.2
0.0
2
3
4
5
6
7
8
9

Fig. 3

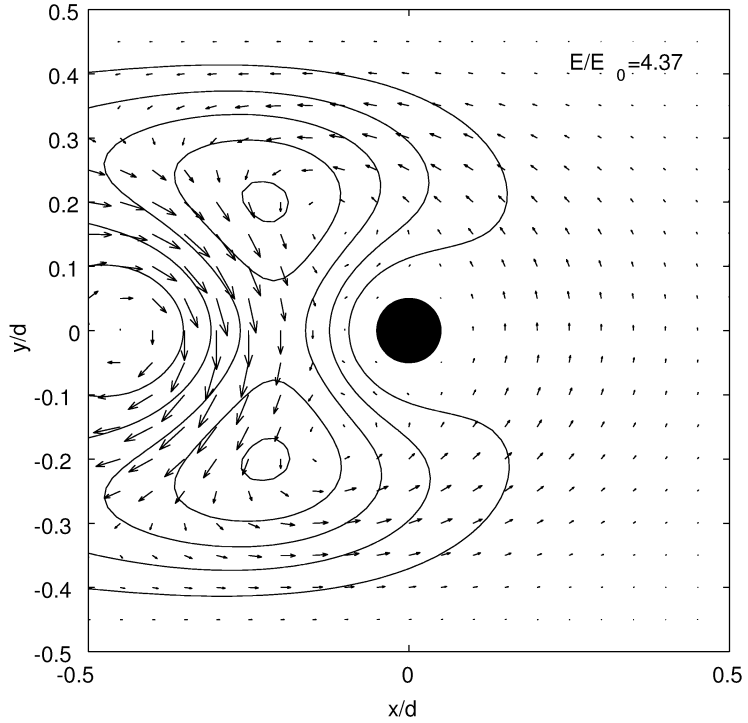
E/E 0=4.37
y/d
x/d
0.5
0.4
0.3
0.2
0.1
0
-0.1
-0.2
-0.3
-0.4
-0.5
-0.5
0
0.5

Fig. 4

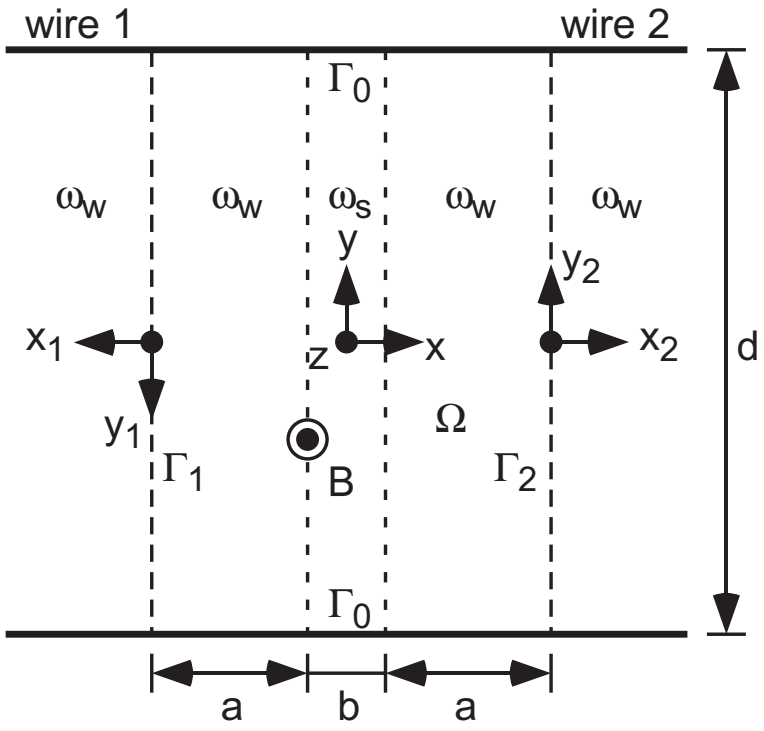
wire 1
wire 2
Γ_0
ω_w
ω_w
ω_s
ω_w
ω_w
y
y_2
x_1
z
x
x_2
d
y_1
Ω
Γ_1
B
Γ_2
Γ_0
a
b
a

Fig. 5

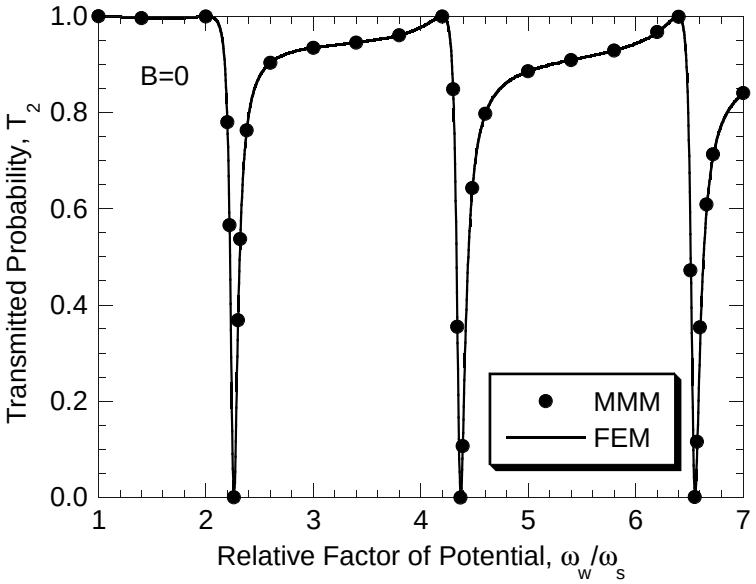
B=0
Transmitted Probability, T_2
Relative Factor of Potential, ω_w/ω_s
MMM
FEM
1.0
0.8
0.6
0.4
0.2
0.0
1
2
3
4
5
6
7

Fig. 6a

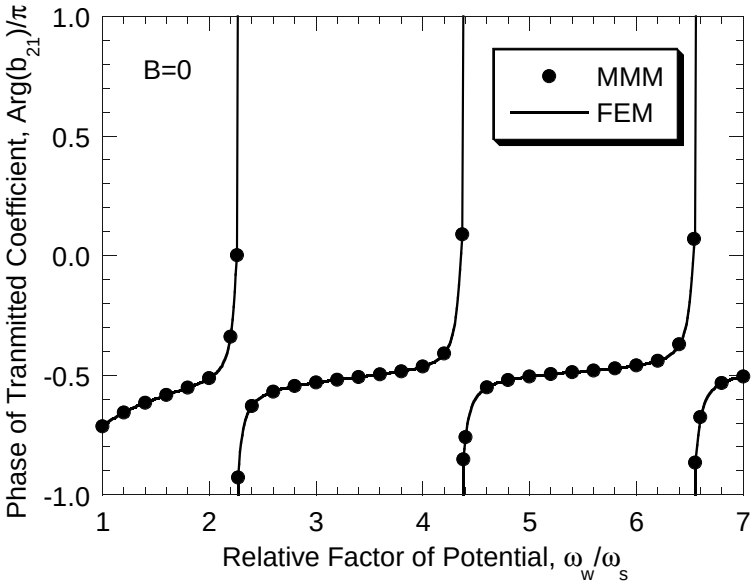
B=0
MMM
FEM
Phase of Tranmitted Coefficient, Arg(b21)/π
Relative Factor of Potential, ω w /ω s
1.0
0.5
0.0
-0.5
-1.0
1
2
3
4
5
6
7

Fig. 6b

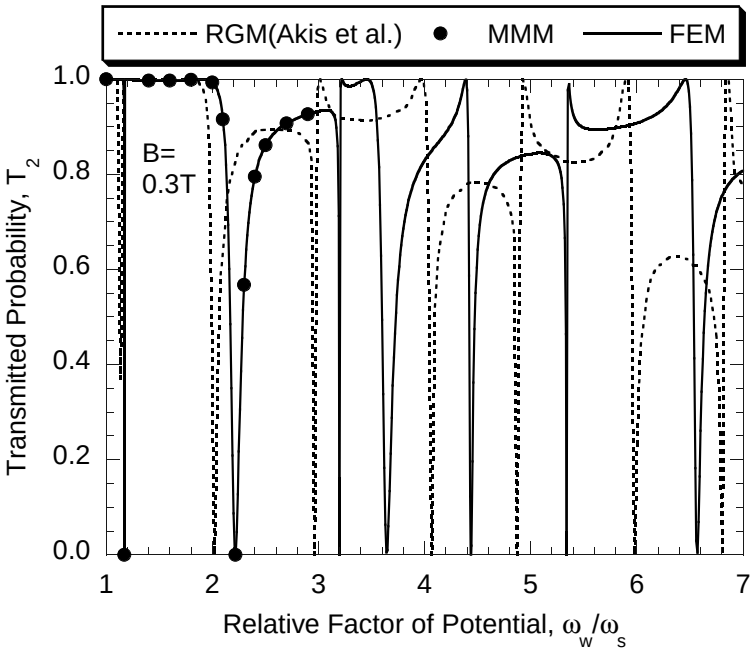
RGM(Akis et al.)
MMM
FEM
B=
0.3T
Transmitted Probability, T2
Relative Factor of Potential, ω w /ω s
1.0
0.8
0.6
0.4
0.2
0.0
1
2
3
4
5
6
7

Fig. 7a

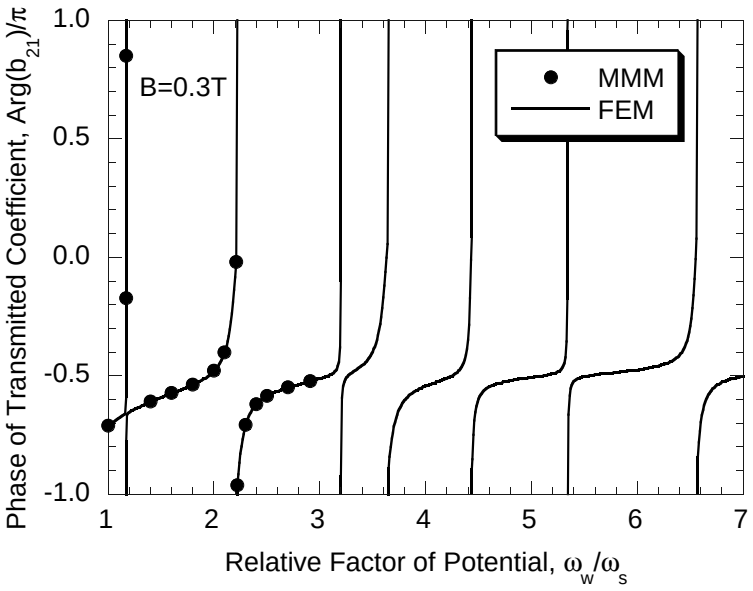

Fig. 7b

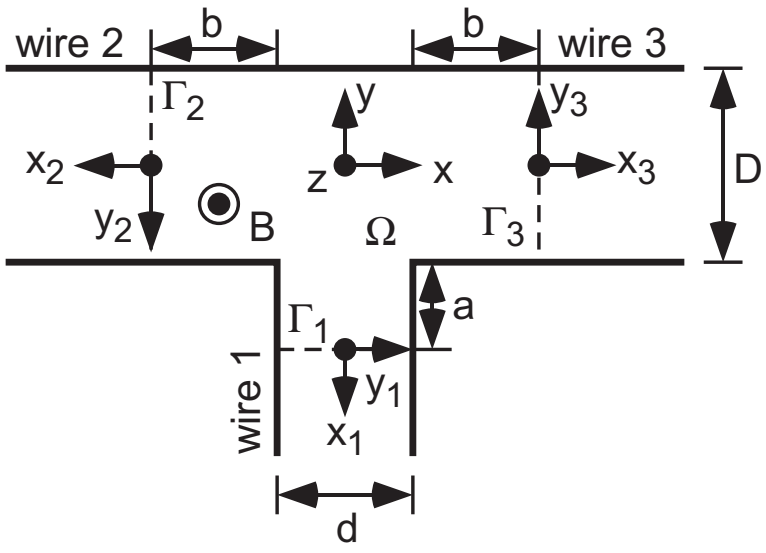

Fig. 8

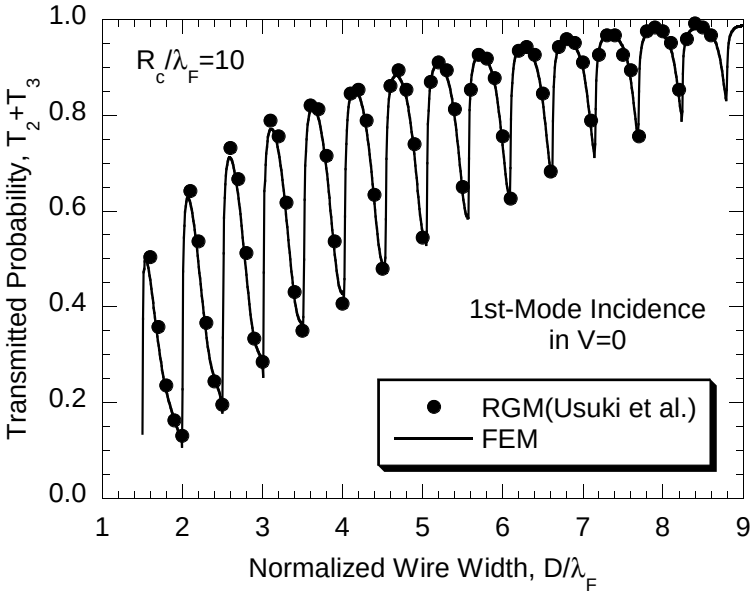

Fig. 9a

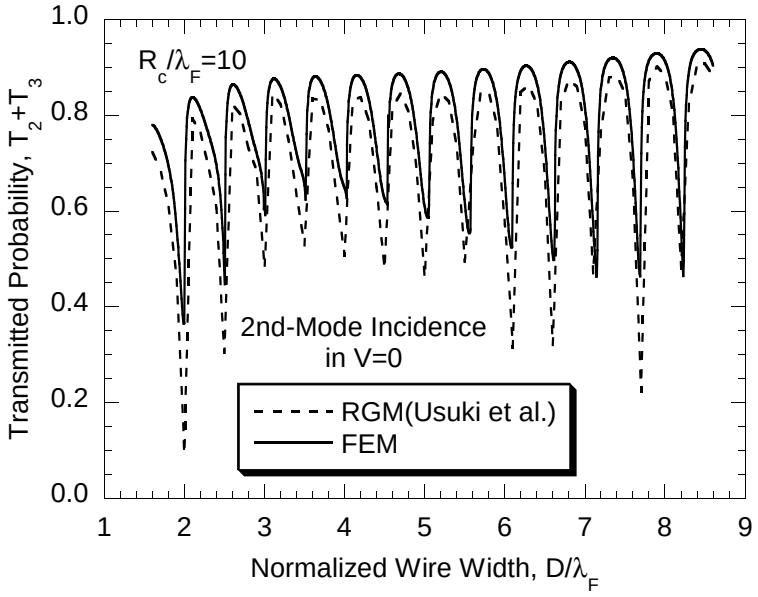
1.0
0.8
0.6
0.4
0.2
0.0
1
2
3
4
5
6
7
8
9
R_c/λ_F=10
2nd-Mode Incidence
in V=0
RGM(Usuki et al.)
FEM
Transmitted Probability, T_2+T_3
Normalized Wire Width, D/λ_F

Fig. 9b

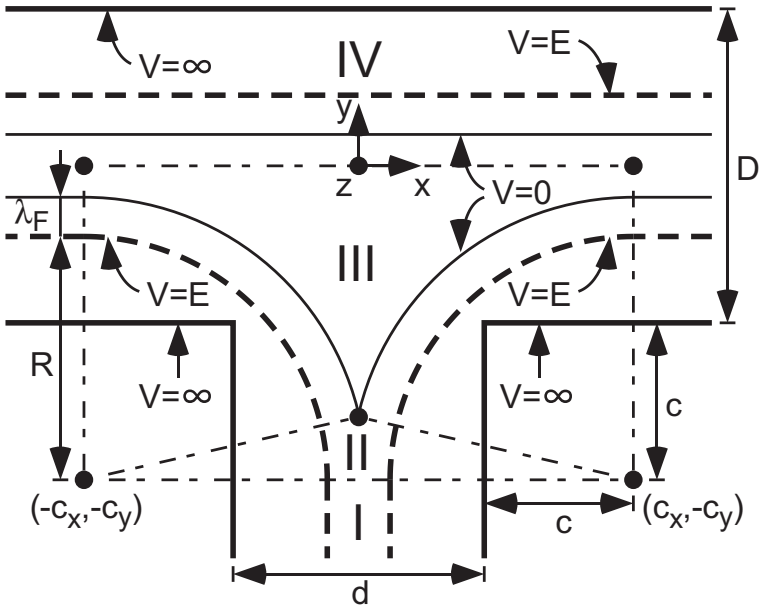
V=∞
IV
V=E
y
z
x
V=0
D
λ_F
III
V=E
V=E
R
V=∞
V=∞
c
II
(-c_x,-c_y)
c
(c_x,-c_y)
I
d

Fig. 10

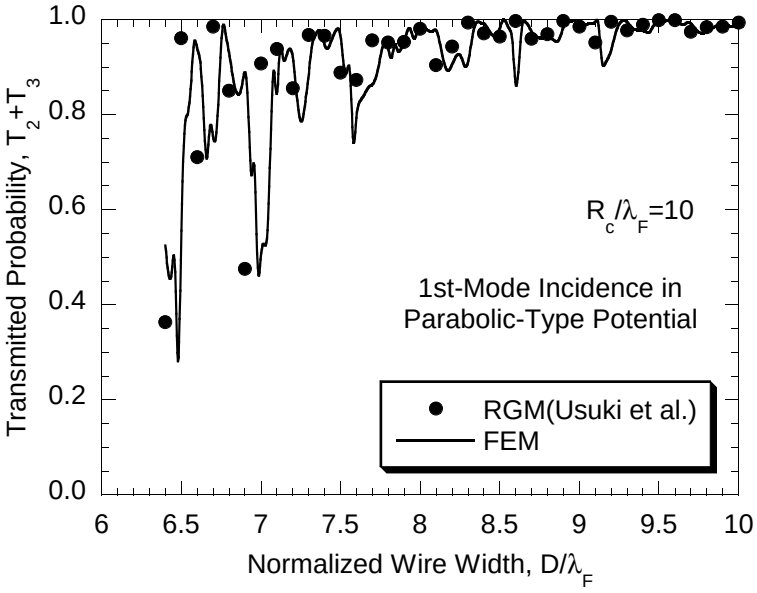

Fig. 11a

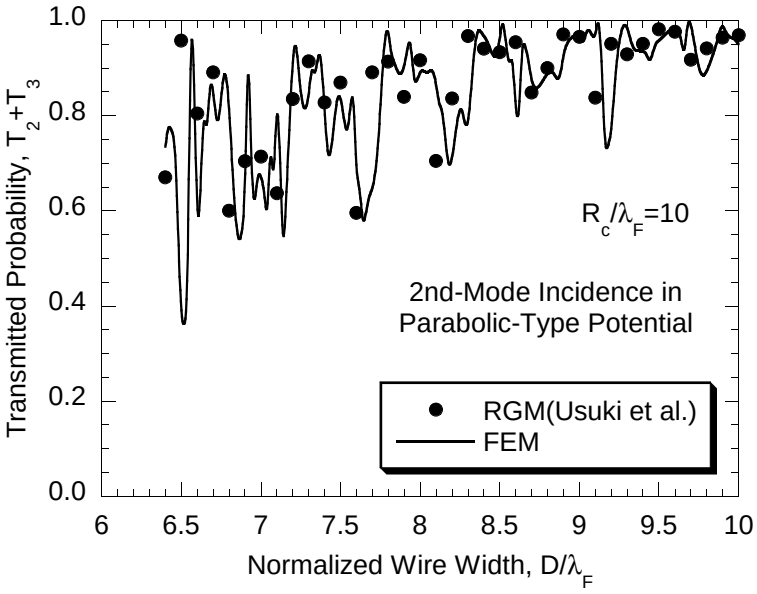

Fig. 11b

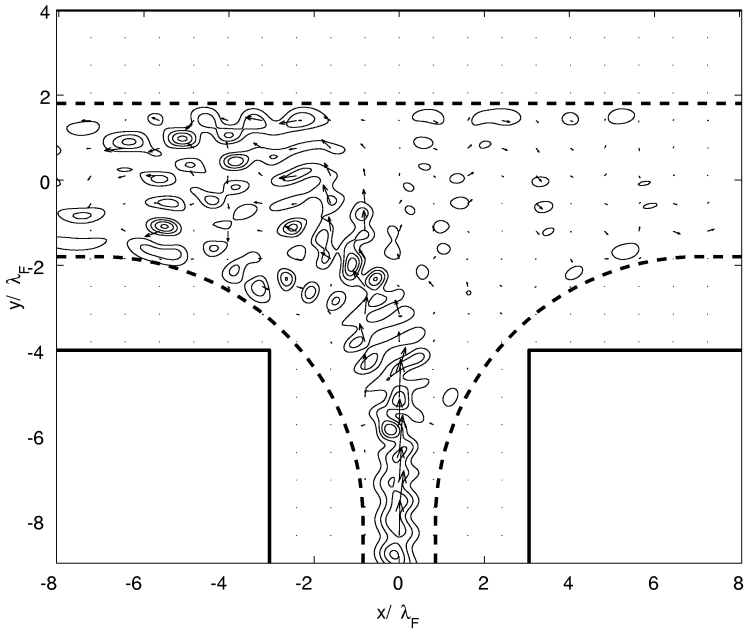

Fig. 12